GEOPHYSICS, VOL. 54, NO. 10 (OCTOBER 1989); P. 1306–1317, 9 FIGS.

Statistically perturbed geophone array responses

David F. Aldridge*

ABSTRACT

Seismic-receiver arrays implemented under typical field conditions are subject to a variety of perturbing influences. The array responses that are actually achieved differ, perhaps substantially, from the nominal response associated with ideal conditions (precise positioning, vertical plants, identical geophones, perfect ground coupling, etc.). Variations in receiver array response may degrade the effectiveness of multichannel processing and analysis schemes that rely upon channel-to-channel waveform constancy. In effect, array-response variation is a form of noise added to recorded waveforms and is thus potentially harmful.

A rigorous physical treatment of the response of a geophone array to incident plane-wave elastic radiation forms the point of departure for assessing the importance of response perturbations. The hard-wired multiple seismometer group, long transmission line, and recording-system input impedance are considered an electromechanical system. An individual geophone may have arbitrarily specified position and axial orientation and is modeled as a ground-motion transducer that incorporates, to first order, the effect of compliant coupling to the earth. Elastic waves (of either vibratory mode) can be incident from any direction. This generality built into the mathematical description of receiver-array response allows numerous array types (including those designed to record shear waves) to be analyzed. All parameters that determine the response value are then subjected to controlled random perturbations in order to evaluate the statistical variability of the complex valued array-response function. Transformation of the perturbed responses to the time domain indicates the extent of waveform variability induced by geophone-array diversity.

Computational studies indicate that, for vertical or near-vertical plane *P*-wave incidence, reasonable variations in the controlling parameters do not reduce waveform coherence by any major amount. Peak times of reflection signal recorded on well planted geophone arrays typically vary by up to 4 ms. As the angle of incidence increases or the quality of the field-array implementation degrades, the wavelets exhibit increasing amplitude loss, wave-shape alteration, and incoherence that may affect an interpretation.

INTRODUCTION

Seismic data acquisition, processing, and interpretation procedures could be improved if they were based on exact knowledge of the propagating waveform. However, precise waveform definition is an elusive goal due to the large number of poorly known factors that affect seismic wavelets. Source, propagation, receiver, and instrumentation effects all contribute in varying amounts to the final recorded signal. In this study, computational modeling of land seismic-receiver arrays is used to examine the influence such arrays exert on seismic wavelets. Particular attention is paid to the natural statistical variability associated with field implementation of these arrays, since this can degrade the waveform coherence observed across a recording spread. In effect, receiver-array diversity in the field constitutes a form of noise added to recorded signal and thus is potentially harmful. Statistical modeling of the waveform variability induced by this array diversity can provide useful information for judging the accuracy and stability of data processing operations such as array-response deconvolution, first-break picking, amplitude-versus-offset analysis, and residual statics calculation. Modeling can also assist in specifying rational recording standards for data acquisition contracts. Ulti-

Presented at the 1988 National Convention, Canadian Society of Exploration Geophysicists. Manuscript received by the Editor September 21, 1988; revised manuscript received March 29, 1989.
*Department of Geophysics and Astronomy, University of British Columbia, 129-2219 Main Mall, Vancouver, B.C., Canada V6T 1W5.

mately, such studies are an attempt to address the fundamental question: "What is the seismic waveform?"

Extended receiver arrays are commonly designed to suppress coherent noise in the seismic record arising from ground roll and other predominantly horizontally traveling energy. If the geophone spacing is large enough, random noise is reduced simultaneously. The array is considered a wavenumber (or wavelength) filter. Design philosophy generally consists of choosing the number of elements, their spatial distribution, and associated multiplicative weights in order to approximate a desired wavenumber response spectrum sufficiently accurately. In a well known computational study, Newman and Mahoney (1973) demonstrated that small random errors in the element positions and weights can cause the array amplitude response to deviate significantly from the theoretical prediction. Arrays requiring very precisely specified weights in order to achieve a low reject-band level were found to be especially intolerant of such errors; the rejection ratio defaulted to a value well below the design criterion. The wavenumber-response spectra display a rather alarming amount of random diversity that prompts the following question: to what extent are the time-domain waveforms filtered by these arrays adversely affected by such errors? After all, the time-domain traces are what are ultimately interpreted for subsurface structure or stratigraphy.

An alternative conception of the receiver array is used here in an attempt to answer this question. The array is considered to be a multichannel input/single-channel output time-domain filter. The complex-valued frequency response of this filter is obtained by analytical techniques after an appropriate model is adopted for seismic wave propagation. Multiplication of this response by the spectrum of an incident seismic signal, followed by inverse Fourier transformation, yields a simulated time-domain waveform output by the array. This simple processing sequence is used to directly assess the effects on the seismic wavelet of the many parameters that control array response.

Smith (1956), Schoenberger (1970), and Newman and Mahoney (1973) have all presented theoretical calculations on the amount of wavenumber rejection an array can practically achieve when element weights are subject to uncertainty. These investigators used a mathematical model of the receiver array consisting of a finite set of weighted and shifted Dirac delta functions. The distribution of the delta functions in coordinate space is representative of the actual geophone positions in the field. Each multiplicative weight assigned to a delta function is really a catchall factor designed to account for various phenomena such as geophone sensitivity, geophone multiplicity at any one location, coupling of the geophone to the ground, electrical weighting of the geophone output voltage, etc. Although the delta-function model is valuable for its conceptual simplicity, it is not a particularly rigorous physical description of how a hard-wired multiple seismometer group actually works. The array model used for the current study is a generalization of that originally developed by Lindsey (1971). The multiple geophone group, long transmission line, and recording system input impedance are treated as an electromechanical system. Electrical interaction among interconnected seismometers is thus accounted for automatically. Extensions of the model incorporated into this study allow for arbitrary specification of the spatial position, axial orientation, electromechanical constants, and ground-coupling parameters of *each* geophone of the array. A scheme for relating the array geometry to the group electrical configuration is thus needed and is described in the following sections. The resulting theoretical description of receiver-array response does not possess many of the restricting conditions that are commonly imposed (uniformly gridded geometry, omnidirectional sensors, identical transducers, parallel axial alignment, etc.).

SOURCES OF ARRAY-RESPONSE VARIATION

A theoretical seismic receiver array design can only be imperfectly implemented in the field. Newman and Mahoney (1973) ably summarize the many perturbing influences that an array is typically subject to. Some of these are briefly restated here. Geophones are not identical transducers but possess some intrinsic electromechanical variability due to finite tolerances associated with the manufacturing process. This variability can be expected to increase after a period of field service. Actual geophone positions can be displaced, in any or all of three dimensions, from their intended locations. Geophone axial orientations are never exactly parallel but are subject to some statistical scatter about the preferred direction. The magnitude of this scatter, as well as the quality of the coupling of the geophones to the ground, is strongly dependent upon the care exercised by the field layout crew in its work. Newman and Mahoney refer to this class of perturbations as "implementation errors." Even if the model adopted for incident seismic wave propagation is rigorously correct, the theoretical array response can never be achieved in practice because the array cannot be deployed exactly as designed.

A second class of errors relates to the mathematical form assumed for the incident seismic signal. In this study, incident radiation consists of plane elastic (not acoustic) waves propagating in a uniform half-space with a stress-free plane boundary. Within the confines of this model, it is possible to discuss array-response variations arising from changing direction, speed, and polarization of the incident waves. For example, the *P*-wave and *S*-wave velocities of the near-surface material upon which arrays are sited may vary along a seismic line. Similarly, the inline or crossline emergence angle of primary reflected signal from a target zone of interest may change from station to station. These factors can yield a changing wavelet among the traces of a gather.

Obviously, real-world departures from this simple model alter the actual array response from the theoretical description. Analysis of effects associated with curved wavefronts, velocity and density heterogeneity, anisotropy, anelastic losses, or reflection from a nonplanar free surface would require a correspondingly more sophisticated model. Newman and Mahoney designate this class as "errors in design assumptions" and make the interesting observation that they may be represented as "equivalent implementation errors" introduced into calculations that employ a simpler wave-propagation model.

RECEIVER-ARRAY GEOMETRY

Consider a set of N_g geophones connected together in some, as yet unspecified, electrical configuration to form a group. The geometry of this receiver array is completely described by specifying the positions and orientations of all geophones in three-dimensional (3-D) space. If **ijk** is an orthonormal triad of basis vectors for a rectangular Cartesian coordinate system, then the position vector $\mathbf{r}_n$ and sensitivity axis $\mathbf{a}_n$ of the nth geophone of the array ($n = 1, 2, \ldots N_g$) are

$$\mathbf{r}_n = x_n\mathbf{i} + y_n\mathbf{j} + z_n\mathbf{k}, \tag{1}$$

$$\mathbf{a}_n = (\sin\alpha_n \cos\beta_n)\mathbf{i} + (\sin\alpha_n \sin\beta_n)\mathbf{j} + (\cos\alpha_n)\mathbf{k}. \tag{2}$$

(x_n, y_n, z_n) are the spatial coordinates of the geophone and (α_n, β_n) are polar and azimuthal angles, respectively, that determine the orientation of its sensitivity axis. The dimensionless unit vector $\mathbf{a}_n$ defines the directional sensing characteristic of the geophone. Ideally, the geophone responds only to the component of elastic particle velocity parallel to its sensitivity axis. However, a practical geophone outputs a small signal in response to motion perpendicular to $\mathbf{a}_n$. No attempt is made to model such crosstalk here.

As an example, the geometry of the commonly used line array of equispaced vertical component geophones is parameterized by $x_n = x_1 + (n-1)d$, $y_n = z_n = 0$, $\alpha_n = 0°$, β_n is arbitrary, where $x_1 = -(N_g - 1)d/2$ and d is the adjacent geophone spacing. This specification locates the coordinate origin O at the center of the array (as is typically assumed for seismic data processing purposes). If the line of profiling is taken to be coincident with the x-axis, then the horizontal radial (or inline) component of ground motion is measured if $\alpha_n = 90°$ and $\beta_n = 0°$; the horizontal transverse (or crossline) component is measured if $\alpha_n = 90°$ and $\beta_n = 90°$.

INCIDENT SEISMIC SIGNAL

Seismic radiation incident upon the receiver array is presumed to consist of plane elastic waves propagating in a homogeneous and isotropic half-space. Use of a half-space earth model allows free-surface effects to be incorporated explicitly into the array-response calculation. In particular, the elastic particle velocity at position **r** and time t is a composite of three terms: the direct arrival and the reflected-mode and converted-mode arrivals generated by the overlying half-space surface (referred to by subscripts d, r, and c, respectively, in subsequent equations). Each term can be expressed as a plane wave propagating with speed V in the direction of a unit vector **n** and polarized in the direction of a unit vector **p**. The propagation direction of the incident direct radiation is defined in terms of polar and azimuthal angles (ϕ, θ) depicted in Figure 1a. Let the surface of the half-space be parallel with the xy plane and intersect the z-axis at (0, 0, h) with $h \geq 0$. Then the elastic particle velocity is

$$\dot{\mathbf{u}}(\mathbf{r}, t) = \mathbf{p}_d s_d\left(t - \frac{\mathbf{r}\cdot\mathbf{n}_d}{V_d}\right) + \mathbf{p}_r s_r\left(t - \frac{\mathbf{r}\cdot\mathbf{n}_r}{V_r} - \frac{2h\cos\phi}{V_r}\right) + \mathbf{p}_c s_c\left[t - \frac{\mathbf{r}\cdot\mathbf{n}_c}{V_c} - h\left(\frac{\cos\phi}{V_d} + \frac{\cos\psi}{V_c}\right)\right], \tag{3}$$

where $s_d(t)$, $s_r(t)$, and $s_c(t)$ are the direct, reflected, and converted particle-velocity waveforms. The angle ψ in the third term of this equation is the incidence angle of converted-mode radiation and is related to that of the direct arrival via Snell's law: $\sin\psi = (V_c/V_d)\sin\phi$. Since the coordinate origin O is a reference point for specification of a particle-velocity signal input to the receiver array, the ability to locate it *below* the half-space surface ($h > 0$) in the above manner is useful in the analysis of buried or downhole arrays.

Two distinct cases of the general equation (3) need to be examined: direct P waves ($V_d = V_r = V_P$, $V_c = V_S$) and direct S waves ($V_d = V_r = V_S$, $V_c = V_P$). Expressions for the unit propagation and polarization vectors appropriate for each situation are given in Appendix A. For plane compressional waves, these vectors are parallel. For plane shear waves, an additional variable is required to characterize polarization perpendicular to the propagation direction. S-type motion is commonly decomposed into uncoupled SH and SV components. Referring to Figure 1b, I define a polarization angle δ with range $0° \leq \delta \leq 90°$. $\delta = 0°$ implies pure SH motion, whereas $\delta = 90°$ implies pure SV motion. For $0° < \delta < 90°$, the incident S wave is a mixture, in varying proportions, of both SH and SV components.

The reflected and converted-mode waveforms are scaled versions of the direct waveform $s_d(t)$ and are also given in Appendix A. Multiplicative scalars involve the four free-surface reflection coefficients for particle velocity: $\acute{P}\grave{P}$, $\acute{P}\grave{S}$, $\acute{S}\grave{P}$, and $\acute{S}\grave{S}$, referred to as the P to P, P to SV, SV to P, and SV to SV coefficients, respectively (the SH to SH coefficient always equals 1.0). These are functions of the direct-wave incidence angle ϕ and the P- and S-wave speeds V_P and V_S of the elastic medium. Numerous functional forms exist (Červený and Ravindra, 1971, p. 66; Aki and Richards, 1980,

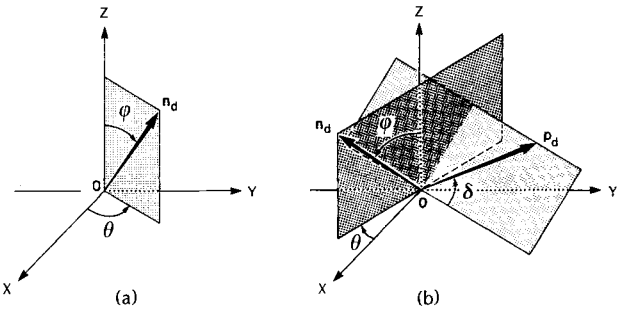

FIG. 1. Incident seismic signal. (a) Unit propagation vector $\mathbf{n}_d$ of incident direct radiation. For direct P waves, this vector is also the unit polarization vector. (b) Relation of unit polarization vector $\mathbf{p}_d$ of direct S waves to propagation vector $\mathbf{n}_d$.

p. 140), but care must be exercised in their use, since inertial and ray-centered coordinate systems describing the particle-motion components tend to vary. The time-domain development outlined here is adequate to handle all free-surface plane-wave reflection problems *except* supercritically incident *SV* waves ($\phi > \sin^{-1} V_S/V_P$). Such arrivals generate phase-shifted reflected *SV* waves and inhomogenous converted *P* waves; the relevant reflection coefficients are complex-valued, frequency-dependent, and applicable in the Fourier frequency domain. Analysis of array response to these arrivals is not undertaken here. Finally, if the free-surface reflection coefficients are set to zero, equation (3) reduces to the expression appropriate for plane elastic waves propagating in a whole space. Most receiver-array response calculations are founded, either explicitly or implicitly, upon this simple earth model.

The set of particle-velocity components detected by a spatially distributed multiple geophone array is found by evaluating equation (3) at each geophone location $\mathbf{r}_n$ and then taking the vector dot product with the respective geophone sensitivity axis $\mathbf{a}_n$:

$$\mathbf{a}_n \cdot \dot{\mathbf{u}}(\mathbf{r}_n, t) = (\mathbf{a}_n \cdot \mathbf{p}_d) s_d \left(t - \frac{\mathbf{r}_n \cdot \mathbf{n}_d}{V_d} \right) + (\mathbf{a}_n \cdot \mathbf{p}_r) s_r \left(t - \frac{\mathbf{r}_n \cdot \mathbf{n}_r}{V_r} - \frac{2h \cos \phi}{V_r} \right) + (\mathbf{a}_n \cdot \mathbf{p}_c) s_c \left[t - \frac{\mathbf{r}_n \cdot \mathbf{n}_c}{V_c} - h \left(\frac{\cos \phi}{V_d} + \frac{\cos \psi}{V_c} \right) \right],$$

$$n = 1, 2, \ldots N_g. \tag{4}$$

Dot products appearing on the right-hand side of this equation can be evaluated from the expressions given in Appendix A. The manner in which these N_g velocity components are now combined to generate the array output voltage depends on two general factors: (1) the electrical interconnection scheme of the geophone group and (2) the transduction characteristics of each seismometer.

GEOPHONE-GROUP FREQUENCY RESPONSE

Lindsey (1971) emphasized that the hard-wired multiple seismometer group, long transmission line, and recording-system input impedance form an electromechanical system that contributes a significant portion of the total filtering applied to the incident ground-velocity signal before it is recorded. He also elucidated a technique, based upon equivalent electrical-circuit principles, for obtaining the frequency response of this multiparameter filter. In this section, Lindsey's method of solution is extended to accommodate receiver groups consisting of nonidentical geophones. This generalization is necessary for studying variations in receiver-array response arising from variability (statistical or otherwise) in the electromechanical and/or ground-coupling characteristics of the individual seismometers.

Figure 2a depicts a group of geophones electrically connected in an M series by N parallel rectangular configuration. The geophone occupying row position i and column position j in this grid is represented by a box enclosing indices i and j. $Z_L(f)$ is the total load impedance presented to the group by the recording channel. In order to facilitate electric-circuit analysis, each geophone is replaced by its Thévenin equivalent circuit consisting of a series combination of an impedance $Z_{ij}(f)$ with an emf $E_{ij}(f)$. Appendix B gives expressions for these quantities appropriate for the moving-coil electrodynamic seismometer. In particular, the emf $E_{ij}(f)$ is related to the ground-velocity component applied to the nth geophone. Standard rules for series and parallel combination of impedances and emfs are then used to reduce the $M \times N$ rectangular grid to its Thévenin equivalent form, Figure 2c. The group equivalent impedance and emf are

$$\frac{1}{Z_G(f)} = \sum_{j=1}^{N} \left[\frac{1}{\sum_{i=1}^{M} Z_{ij}(f)} \right], \tag{5}$$

and

$$E_G(f) = \sum_{j=1}^{N} \left[\frac{Z_G(f)}{\sum_{i=1}^{M} Z_{ij}(f)} \right] \left[\sum_{i=1}^{M} E_{ij}(f) \right]. \tag{6}$$

The complex load current $I_L(f)$ is now easily obtained by applying Kirchhoff's second law around the single equivalent-circuit loop. The load voltage $E_L(f)$ is

$$E_L(f) = I_L(f) Z_L(f) = \left[\frac{Z_L(f)}{Z_L(f) + Z_G(f)} \right] E_G(f). \tag{7}$$

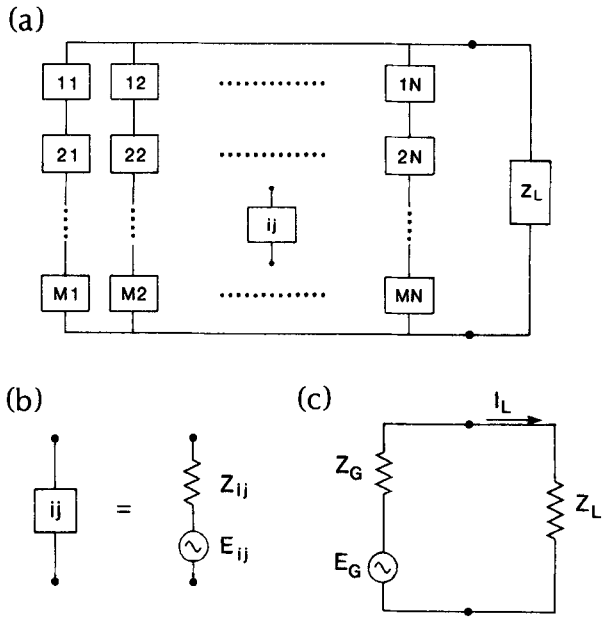

FIG. 2. Series-parallel group connection. (a) $M \times N$ rectangular grid. Z_L is total load impedance presented to geophone group. (b) Thévenin equivalent circuit for a geophone. (c) Thévenin equivalent circuit for a geophone group.

Finally, multiplication of $E_L(f)$ by the appropriate transfer factor $T(f)$ yields the (Fourier transformed) voltage $E_R(f)$ appearing across the recording system input impedance:

$$E_R(f) = T(f)E_L(f) = \left[\frac{T(f)Z_L(f)}{Z_L(f) + Z_G(f)}\right]E_G(f). \qquad (8)$$

When all of the geophones are identical [$Z_{ij}(f) = Z(f)$], expression (8) reduces to a form consistent with equation (5) in Lindsey (1971) when the appropriate notational conversions are made. Expressions for the group load impedance $Z_L(f)$ and voltage transfer factor $T(f)$ are given in Appendix C.

The relationship between the electrical configuration and the spatial distribution of the geophones is defined by requiring the indices i and j to be integer valued functions of the position index n used in the previous section:

$$i = i(n) \qquad (i = 1, 2, \ldots M),$$

$$j = j(n) \qquad (j = 1, 2, \ldots N),$$

with $n = 1, 2, \ldots N_g$, and $N_g = MN$. Unambiguous specification of this relationship is essential if the individual geophone electromechanical and/or ground coupling parameters are not precisely the same.

No assumptions have yet been made regarding the explicit functional forms of the individual geophone impedances $Z_{ij}(f)$ or emfs $E_{ij}(f)$. A beneficial consequence of this generalized point of view is that the above equations describing group frequency responses are valid for *any* type of seismometer as long as the Thévenin equivalent representation is valid. Calculation of the group response merely requires that the appropriate forms for equivalent impedance and emf be derived. Hence, the above analysis applies to more novel transducer designs such as fixed-coil geophones (Kanemori and Hall, 1986) and accelerometers (Klaassen and Van Peppen, 1983), as well as to the standard moving-coil geophone.

STATISTICALLY PERTURBED RESPONSE CALCULATIONS

The preceding sections have developed a deterministic model for the response of a land seismic-receiver array to incident plane elastic waves. Equation (8) is a frequency-domain expression for the recording-system input voltage (i.e., volts per hertz) that can be evaluated after the geophone array and input seismic radiation are well defined. An unambiguous description of the array entails the specification of the following information: (1) the number of geophones; (2) their positions, orientations, electromechanical constants, and ground-coupling parameters; (3) the group electrical configuration; and (4) the load impedance of the recording channel. Incident direct-arriving waves are defined in terms of their propagation direction, polarization, speed, and particle-velocity spectrum. After evaluation of $E_R(f)$ over a suitable frequency range, the time-domain voltage $e_R(t)$ applied to the recording-system input terminals is obtained by inverse discrete Fourier transformation. Of course, in an actual field situation, this voltage is subject to further filtering by the recording instrumentation (including normalization and nondimensionalization in the digitizing process) before being written to tape as a sampled time series.

The array frequency response, defined as the recording-system input-voltage spectrum divided by the direct-arrival particle-velocity spectrum [$E_R(f)/S_d(f)$], is easily obtained by assuming an impulsive incident particle velocity in the calculation [$s_d(t) = \delta(t)$, implying $S_d(f) = 1$]. In any practical seismic reflection experiment, many (or all) of the parameters that determine this response can be considered random variables. The array-response function itself is then a random-valued function of frequency possessing a probability distribution that is related, in a complicated manner, to those associated with the controlling parameters. Due to the nonlinear dependence of the response function upon the many parameters, an analytical derivation of the mathematical form of this distribution would be exceedingly difficult. Furthermore, the probability distributions governing these parameters are unknown. For these reasons, the statistical variability of the geophone-array response function is best examined by conducting numerical Monte Carlo experiments that repeatedly simulate the natural conditions of field-array implementation. This approach retains the advantage of flexibility in the choice of probability distributions to assign to the array-response parameters.

Difficult and unresolved questions exist as to what probability distributions the basic random variables (the array-response parameters) are drawn from and to what extent these random variables are independent. These questions are simply bypassed here and the following utilitarian philosophy adopted: the receiver-array parameters are considered independent random variables drawn from populations that (with the exception of the geophone sensitivity axis $\mathbf{a}_n$) are uniformly randomly distributed, within predefined limits, about their nominal values. The rectangular distribution has the advantage of imposing finite limits on the allowed range of the random variable. This is conceptually and practically desirable in the case of those variables (like geophone electromechanical constants) that must be positive valued.

The geophone sensitivity axis $\mathbf{a}_n$ is a vector-valued random variable assumed to be drawn from a Fisher probability distribution. The Fisher distribution (Fisher, 1953) is widely used in the analysis of rock magnetism data to infer paleomagnetic field direction. Measured remanent magnetization directions from a set of rock samples taken from an outcrop are never identical but are grouped, either closely or loosely, about a preferred direction called the pole. With respect to this pole, a given specimen possesses a polar angle η and an azimuthal angle χ. Fisher proposed that these two angles are independent random variables, that the azimuth angle χ is uniformly distributed over the full 360°, and that the polar angle η has a probability density function given by

$$f(\eta) = \left(\frac{\kappa}{2 \sinh \kappa}\right)e^{\kappa \cos \eta} \sin \eta, \qquad 0 \le \eta \le \pi. \qquad (9)$$

κ is an invariance (reciprocal variance) parameter. For $\kappa = 0$, the angular probability density function becomes $(\sin \eta)/2$, representing an isotropic distribution of the unit-direction vectors in 3-D space. As $\kappa \to \infty$, $f(\eta)$ approaches $\delta(\eta)$, corresponding to perfect alignment of the sample directions with the pole. In the context of geophone planting, the pole

direction becomes the intended orientation of the geophones (straight up for vertical-component geophones); the distribution of the actual orientations is rotationally symmetric about this intended direction and governed by the density function (9). Sampling from the Fisher distribution is easily performed on a digital computer. If R is a sample drawn from a rectangular probability distribution on (0, 1), then F, given by

$$F = \cos^{-1}\left\{\frac{1}{\kappa}\ln\left[(1-R)e^{+\kappa} + Re^{-\kappa}\right]\right\}, \qquad (10)$$

is a sample from a population of polar angles distributed according to the Fisher density law.

EXAMPLE I

The two examples discussed in this paper are representative of a large number of computational experiments conducted for the purpose of examining statistically perturbed receiver-array responses. Of particular interest in these experiments were the following two questions: (1) Do typical random variations in the parameters that determine array response unduly reduce the seismic-waveform coherence observed in a trace gather? (2) What is the relative importance of the different classes of controlling parameters in contributing to array-response diversity?

The nominal array of the first example is a line array of nine equispaced, vertical-component geophones sited on the surface of an elastic half-space. An element spacing of 2 m implies a moderately high-resolution reflection experiment. The geophones are LRS-1011 models with electromechanical constants ($M, f_0, h_{oc}, G, R_c, L_c, R_s$) given by (0.0079 kg, 14 Hz, 0.48, 27.56 V/m/s, 420 Ω, 0.015 H, 3000 Ω). The group electrical configuration is a 3 × 3 square grid and recording-channel load is provided by the input impedance of a DFS-VII distributed acquisition system (20 kΩ in parallel with 0.01 μF). No extended transmission line effects are included in the calculations. Initially, the geophones are considered to be perfectly rigidly coupled to the half-space surface. Rigid coupling is easily simulated by setting the coupling natural frequency f_g to a value well above the frequency band of interest.

Direct-arriving plane P waves are restricted to vertical incidence for this example. Although this is an idealization, it is nevertheless the desired situation for primary reflections from the target zone of interest. For such normal incidence, the array-response function is insensitive to variations in the horizontal positions of the geophones and the P-wave and S-wave speeds of the elastic medium.

Each frame of Figure 3 displays 25 replications of array amplitude or phase response obtained by randomizing certain classes of parameters. In Figure 3a the seven electromechanical constants of each geophone are subject to uniform random variations limited at ±10% of their nominal values. Specification sheets published by geophone manufacturers cite tolerances associated with these components that typically range from ±5% to ±15% of the stated nominal values. Shapes of the calculated amplitude responses are virtually identical. The loss in amplitude at low frequencies is associated with the transduction property of the geophones. On their flat portions, the curves exhibit only ±5% scatter in amplitude level. Phase response curves show a remarkable stability; the maximum spread among curves is 5° in the vicinity of the geophone natural frequency.

The effect of randomizing geophone orientations is displayed in Figure 3b. The nine geophone sensitivity axes are drawn from a Fisher distribution with invariance parameter $\kappa = 20$. The theoretical mean and standard deviation of the random polar angles α_n implied by this invariance value are 16° and 8.5°, respectively. A careful measurement indicates that the overall level of the amplitude response curves is depressed, relative to that of Figure 3a, by a factor closely equal to cos 16° = 0.94, as expected. Perhaps surprisingly, the scatter in the amplitude response curves is only ±3%, less than that of Figure 3a. Phase responses are unaffected by the randomized orientations because of the assumed normal incidence for the elastic radiation. In general, for oblique plane-wave incidence or for geophones not constrained to reside on the surface, the array phase response would be altered by changing the direction of any geophone sensitivity axis.

A compliant ground coupling is introduced into the problem in Figure 3c by setting the coupling natural frequencies and damping factors equal to 250 Hz and 0.5, respectively. Uniform random variation limited at ±20% of these values is then allowed in order to simulate a fairly wide range of coupling conditions. Extensive field and laboratory measurements of the geophone ground-coupling phenomenon reported by Krohn (1984) suggest that these values are quite reasonable for vertical-component seismometers planted on

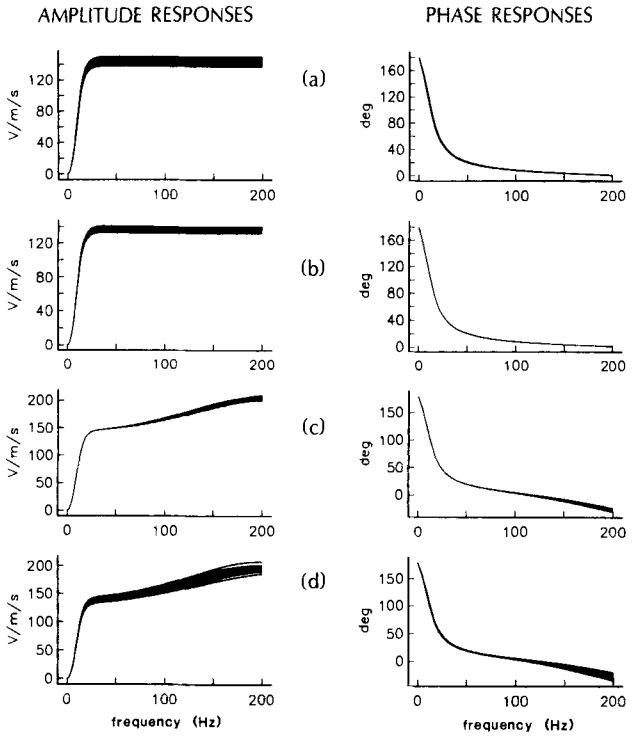

FIG. 3. Statistically perturbed responses for vertically incident P waves. (a) Geophone electromechanical constants randomized. (b) Geophone orientations randomized. (c) Ground-coupling parameters randomized. (d) Simultaneous randomization of electromechanical constants, orientations, and ground-coupling parameters. 25 replications of amplitude or phase response are plotted in each frame.

the surface. The statistical variation of coupling within the arrays induces a diversity into the high-frequency portion of the response curves that, for conventional recording bandwidths, should not create any problems. Comparison of Figures 3b and 3c verifies Krohn's (1984) speculation that the effects of varying geophone orientation are more significant than coupling effects at typical seismic reflection frequencies. Of course, this conclusion rests upon the assumption that the geophone array is well coupled to the ground.

Finally, simultaneous randomization of the geophone electromechanical constants, orientations, and ground-coupling parameters using the previously cited limits yields the amplitude and phase response curves of Figure 3d. The amount of waveform variability created within a trace gather by this level of response-function diversity is now quantified by filtering these array responses with an input particle-velocity spectrum and inverse Fourier transforming. The direct-arrival waveform depicted in Figure 4a is a Berlage (1930) wavelet of the form

$$s_d(t) = AH(t)t^n e^{-\alpha t} \cos(2\pi f_0 t + \phi_0), \qquad (11)$$

where $H(t)$ is the Heaviside unit step function. This pulse is a realistic approximation to many physical seismic wavelets; in particular, a suitable selection of the parameter values in equation (11) yields the common "cycle and a half and not much more" character. Furthermore, the Berlage wavelet spectrum is easily obtained by analytical techniques for evaluation over the desired frequency range. The suite of amplifier input voltages obtained by the aforementioned process is depicted in Figure 4b. Although there are small amplitude and phase differences among the waveforms, the overiding impression is one of very high coherency. The semblance coefficient of these traces, calculated over the displayed 100 ms time window, exceeds 0.99945. If we adopt the usual model of a trace gather as an additive composition of common signal with uncorrelated noise, then the signal-to-noise ratio (defined as the signal energy divided by the mean noise energy) implied by this semblance value is 1765. Evidently, variation of these array-response parameters in concert is an insignificant contributer to seismic-waveform incoherence. This example reveals that the influence of the electromechanical constants is approximately the same as that of the geophone orientations.

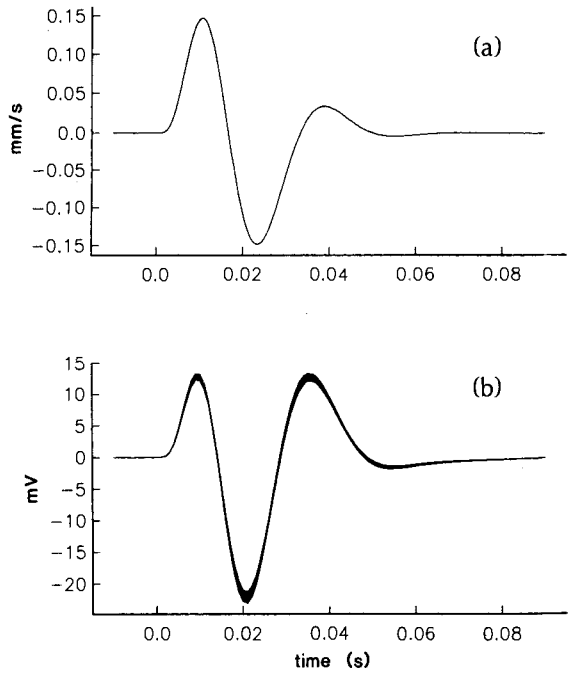

FIG. 4. (a) Particle velocity waveform of incident direct wave is a Berlage wavelet with constants $A = 10^6$ mm/s^4, $n = 3$, $\alpha = 188.5$ rad/s, $f_0 = 30$ Hz, and $\phi_0 = -\pi/2$. (b) 25 replications of recording-system input voltage generated by the perturbed array responses of Figure 3d.

EXAMPLE II

The array geometry of the second example is taken from a recent Western Canadian vibroseis survey. Eighteen vertical-component geophones, spaced at 4.44 m, are arranged in a line array on a half-space surface. Individual geophones are Sensor SM-7B models with $(M, f_0, h_{oc}, G, R_c, L_c, R_s)$ equal to (0.011 kg, 10 Hz, 0.25, 28.8 V/m/s, 375 Ω, 0.02 H, 1000 Ω); coupling frequencies and damping factors are again taken to be 250 Hz and 0.5, respectively. The 9 × 2 series-parallel hookup is connected directly to the recording system used in the previous example. Inline plane P waves are incident at a shallow angle from the vertical [$(\phi, \theta) = (12°, 0°)$]. Wave speeds of the elastic medium are $V_P = 1000$ m/s and $V_S = 577$ m/s, corresponding to a Poisson's ratio of 0.25.

Figure 5a displays perturbed responses obtained by simultaneously varying geophone horizontal positions, orientations, electromechanical constants, and ground-coupling parameters. The major effects within the first lobe of the amplitude responses are due to electromechanical constants and orientations, contributing in about equal amounts. Variation of positions and ground-coupling parameters affect only higher frequency lobes significantly. Unwrapped phase curves in Figure 5a exhibit rapid changes of approximately ±180° in the vicinity of the amplitude-spectrum notches. These abrupt, but nevertheless continuous, changes are induced by zeros of the complex-valued response function shifting away from the real-frequency axis. If a zero shifts into the lower half-plane, a −180° phase change is induced, and the associated time-domain impulse response cannot be minimum phase.

The effects of varying the elastic-wave speeds and the direction of incident radiation are depicted in Figures 5b and 5c, respectively. To first order, these array-response spectra are stretched or compressed versions of the nominal spectrum. The small amount of amplitude diversity visible in Figure 5b is due to the changing free-surface reflection coefficients $\acute{P}\grave{P}$ and $\acute{P}\grave{S}$. The ±5% variation in V_P and V_S might be typical of the nonuniformity in near-surface velocities appearing across a recording spread length. Similarly, refraction of incoming rays through the variable base of the weathered zone can result in a changing incidence angle, in both the inline and crossline directions, of primary reflected energy from the target zone. A somewhat higher level of amplitude variation is created by this effect despite the fact that ϕ and θ are varied by only ±2.5° and ±5°, respectively.

Simultaneous randomization of all of the stated parame-

ters yields the response curves of Figure 5d. Both amplitude and phase responses exhibit significant variability beyond the first notch of the amplitude spectrum. These spectra are filtered by multiplying by the Fourier transform of the Klauder wavelet expected for this vibroseis survey. After inverse Fourier transformation, the suite of wavelets in Figure 6b is obtained. A fairly high level of coherence is maintained (S_c = 0.98785, S/N = 78), although some amplitude and phase fluctuations that could be misinterpreted are present. Comparison of Figures 6a and 6b indicates that significant amplitude loss is associated with nonvertical incidence of only 12°. This loss is due primarily to the strong band-limiting effect of the extended array on the incident pulse.

The magnitudes of the parameter perturbations applied in examples I and II are considered quite realistic for well planted geophone arrays. Figures 4b and 6b then imply that these variations do not adversely impact traveltime measurements to any large extent. For example, the maximum difference in peak times among the wavelets in Figure 6b is only about 4 ms.

Figure 7 displays wide-angle (ϕ = 30°) inline *P*-wave responses of the example II array. The applied parameter perturbations are identical to those previously used. Three amplitude-spectrum notches (and associated phase-spectrum jumps) appear within the passband of the Klauder wavelet used for filtering. The time-domain waveforms exhibit a further reduction in amplitude level and coherence (S_c = 0.96803, S/N = 29), as well as a marked alteration in waveshape. The maximum difference in peak times is still about 4 ms, but now the peak-to-peak amplitudes vary by approximately ±25% about the average value.

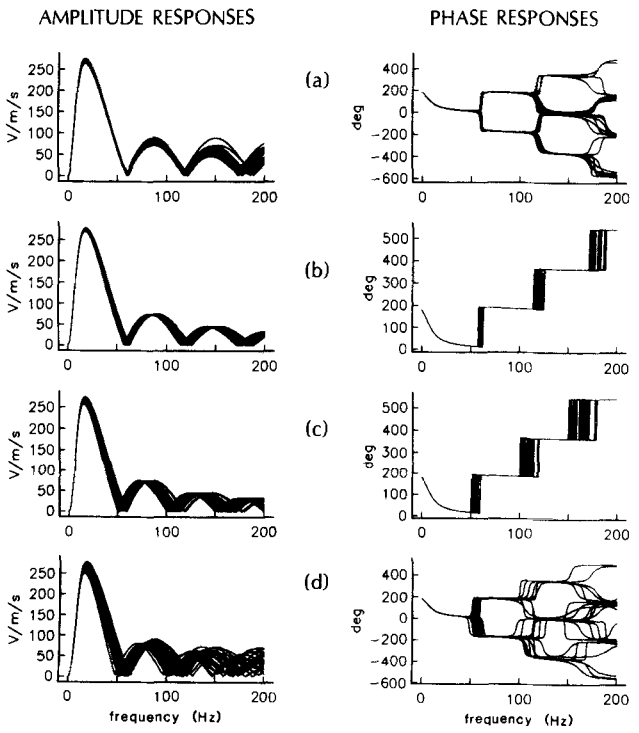

FIG. 5. Statistically perturbed responses for *P* waves incident at an oblique angle. (a) Horizontal positions, electromechanical constants, and ground-coupling parameters randomized by ±0.5 m, ±5%, and ±20%, respectively. Random orientations drawn from Fisher distribution with κ = 75 (mean = 8°, standard deviation = 4°). (b) *P*- and *S*-wave speeds randomized by ±5%. (c) Polar and azimuthal angles of incident waves randomized by ±2.5° and ±5°, respectively. (d) Simultaneous randomization of all parameters by previously stated amounts. 25 array-response replications are plotted in each frame.

CONCLUSION

The mathematical description of land seismic receiver-array response is recast in a form that takes explicit account of the many physical factors known (or presumed) to influence the waveforms recorded by such arrays. The importance of variations in these controlling parameters in contributing to seismic waveform incoherence can then be evaluated directly. The effects of small perturbations in geophone properties (horizontal positions, axial orientations, electromechanical constants, and ground-coupling parameters) and incident plane *P*-wave properties (propagation direction and speed) have been investigated here.

Computational studies indicate that, for vertical or near-vertical plane-wave incidence, reasonable variations in the parameters that determine the geophone-array response function do not reduce waveform coherence by any major amount. Calculated amplitude- and phase-response curves exhibit what appears to be significant variability beyond the first notch of the nominal amplitude spectrum. However,

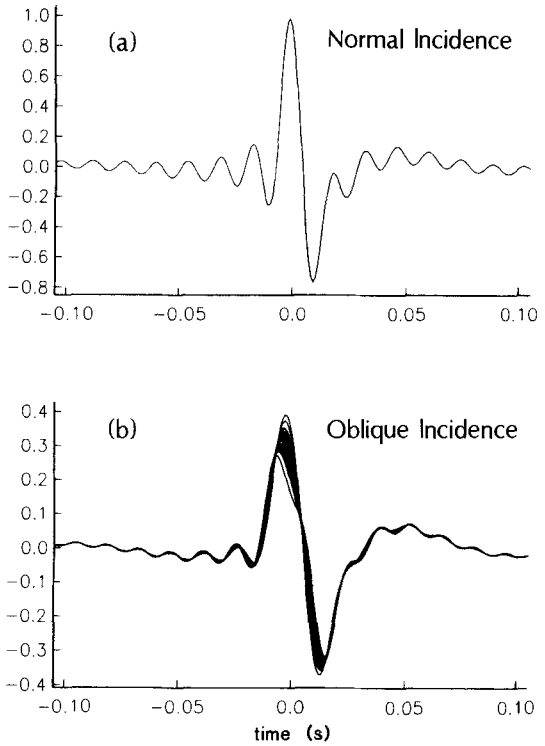

FIG. 6. (a) A Klauder wavelet from a linear vibroseis sweep with bandwidth 8–72 Hz, duration 16 s, and a 0.5 s raised cosine taper has been filtered at vertical incidence by the nominal geophone array of example II. (b) 25 replications of the same Klauder wavelet filtered by the perturbed array responses of Figure 5d. Same vertical scale applies to (a) and (b).

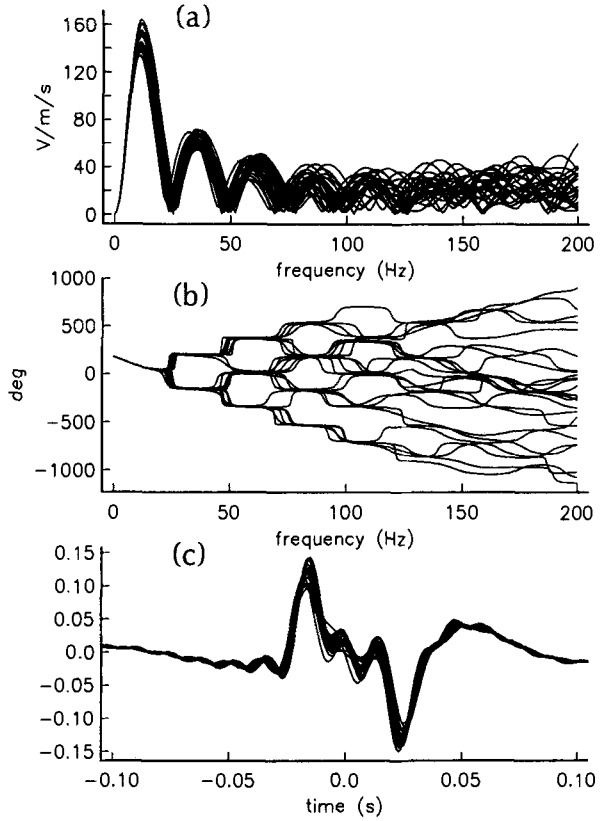

FIG. 7. Statistically perturbed responses for P waves incident at a wide angle from the vertical. All array-response parameters are simultaneously randomized by the amounts used for Figure 5d. (a) Amplitude responses. (b) Phase responses. (c) Klauder wavelets (8–72 Hz) filtered by the responses of (a) and (b). Same vertical scale applies to Figures 6 and 7c. 25 replications are plotted in each frame.

this diversity is not necessarily introduced into the time-domain waveforms filtered by these arrays. The wavelets retain a fairly high degree of coherence if the bandwidth of the incident pulse is predominantly below the first notch frequency. This observation is consistent with computational and theoretical results obtained by Newman and Mahoney (1973) using a simpler receiver-array model. Their amplitude-response spectra (plotted as functions of apparent horizontal wavelength) exhibit an increasing diversity as the wavelength decreases through the first notch value. A corollary of this result is that arrivals incident at a wide angle from the vertical can be subject to a high noise level induced by the array-response variability. Such arrivals can include first breaks (propagating primarily as head waves), shallow interface reflections, steeply dipping interface reflections, far-offset events, and ground roll.

The generality of the derived model of geophone-array response should be of interest to all those who need to design or analyze seismic-receiver arrays. In particular, arrays designed to record S-wave arrivals can be examined with the same techniques as outlined here. It is expected that such arrays will exhibit a greater sensitivity to statistical perturbations of the controlling parameters than P-wave arrays. However, a definitive statement on this situation requires further research.

ACKNOWLEDGMENTS

The author was a Killam predoctoral fellow at the University of British Columbia while conducting this research. Support from NSERC grant 5-84270 is also greatly appreciated. Special thanks are due to Professor Doug Oldenburg for continual encouragement and constructive criticism.

REFERENCES

Aki, K., and Richards, P. G., 1980, Quantitative seismology, theory and methods, **1**: W. H. Freeman and Co.
Berlage, H. P., Jr., 1930, Seismometer, auswertung der diagramme: Handbuch der Geophys., **4**, 299–526.
Berni, A. J., and Parrish, J. F., 1981, Electrical transmission characteristics of marine seismic cable: IEEE Trans. Geosci. Remote Sensing, **19**, 42–46.
Červený, V., and Ravindra, R., 1971, Theory of seismic head waves: Univ. of Toronto Press.
Fisher, R. A., 1953, Dispersion on a sphere: Proc., Roy. Soc. London, Ser. A, **217**, 295–305.
Hoover, G. M., and O'Brien, J. T., 1980, The influence of the planted geophone on seismic land data: Geophysics, **45**, 1239–1253.
Kanemori, T., and Hall, E. M., Jr., 1986, A new type of geophone, eddy-seis, theoretical study of its response characteristics and method of testing: 56th Ann. Internat. Mtg., Soc. Explor. Geophys., Expanded Abstracts, 451–454.
Klaassen, K. B., and Van Peppen, J. C. L., 1983, Electronic acceleration-sensitive geophone for seismic prospecting: Geophys. Prosp., **31**, 457–480.
Krohn, C. E., 1984, Geophone ground coupling: Geophysics, **49**, 722–731.
Lindsey, J. P., 1971, Filtering characteristics of multiple seismometer groups, long cables, and the amplifier input impedance: IEEE, Trans. Geosci. Electron., **9**, 34–42.
Newman, P., and Mahoney, J. T., 1973, Patterns—with a pinch of salt: Geophys. Prosp., **21**, 197–219.
Schoenberger, M., 1970, Optimization and implementation of marine seismic arrays: Geophysics, **35**, 1038–1053.
Smith, M. K., 1956, Noise analysis and multiple seismometer theory: Geophysics, **21**, 337–360.
Smither, M. A., and Khan, T. A., 1983, Modeling the noise pickup of seismic cable: 53rd Ann. Internat. Mtg., Soc. Explor. Geophys., Expanded Abstracts, 460–462.

APPENDIX A

HALF-SPACE WAVE-PROPAGATION FORMULAS

Unit propagation vectors for direct, reflected, and converted plane elastic waves in a half-space are, respectively,

$$\mathbf{n}_d = (\sin\phi\cos\theta)\mathbf{i} + (\sin\phi\sin\theta)\mathbf{j} + (\cos\phi)\mathbf{k}, \quad \text{(A-1)}$$

$$\mathbf{n}_r = (\sin\phi\cos\theta)\mathbf{i} + (\sin\phi\sin\theta)\mathbf{j} - (\cos\phi)\mathbf{k}, \quad \text{(A-2)}$$

and

$$\mathbf{n}_c = (\sin\psi\cos\theta)\mathbf{i} + (\sin\psi\sin\theta)\mathbf{j} - (\cos\psi)\mathbf{k}. \quad \text{(A-3)}$$

ψ is the incidence angle of converted mode radiation and is related to the associated angle for direct waves by Snell's law:

$$\frac{\sin\psi}{V_c} = \frac{\sin\phi}{V_d}, \quad \text{(A-4)}$$

where $V_d = V_P$, $V_c = V_S$ for direct P waves and $V_d = V_S$, $V_c = V_P$ for direct S waves. If supercritical SV waves are excluded from the analysis, ψ is always well defined.

Unit polarization vectors assume different forms depending on whether the direct radiation is compressional or shear mode. For direct P waves,

$$\mathbf{p}_d = \mathbf{n}_d, \tag{A-5}$$

$$\mathbf{p}_r = \mathbf{n}_r, \tag{A-6}$$

and

$$\mathbf{p}_c = (\cos\psi\cos\theta)\mathbf{i} + (\cos\psi\sin\theta)\mathbf{j} + (\sin\psi)\mathbf{k}. \tag{A-7}$$

For direct S waves,

$$\mathbf{p}_d = \cos\delta[(-\sin\theta)\mathbf{i} + (\cos\theta)\mathbf{j}] + \sin\delta[(-\cos\phi\cos\theta)\mathbf{i} + (-\cos\phi\sin\theta)\mathbf{j} + (\sin\phi)\mathbf{k}], \tag{A-8}$$

and

$$\mathbf{p}_r = \frac{\acute{H}\grave{H}\cos\delta[(-\sin\theta)\mathbf{i} + (\cos\theta)\mathbf{j}] + \acute{S}\grave{S}\sin\delta[(\cos\phi\cos\theta)\mathbf{i} + (\cos\phi\sin\theta)\mathbf{j} + (\sin\phi)\mathbf{k}]}{\sqrt{(\acute{H}\grave{H})^2\cos^2\delta + (\acute{S}\grave{S})^2\sin^2\delta}}, \tag{A-9}$$

and

$$\mathbf{p}_c = \mathbf{n}_c. \tag{A-10}$$

Dot products appearing on the right-hand side of equation (4) can be easily written in terms of the above expressions.

Reflected and converted particle-velocity waveforms are scaled versions of the direct waveform. For direct P waves,

$$s_r(t) = \acute{P}\grave{P}s_d(t) \tag{A-11}$$

and

$$s_c(t) = \acute{P}\grave{S}s_d(t). \tag{A-12}$$

For direct S waves,

$$s_r(t) = \sqrt{(\acute{H}\grave{H})^2\cos^2\delta + (\acute{S}\grave{S})^2\sin^2\delta}\,s_d(t) \tag{A-13}$$

and

$$s_c(t) = \acute{S}\grave{P}\sin\delta\,s_d(t). \tag{A-14}$$

$\acute{H}\grave{H}$ is the SH to SH particle-velocity reflection coefficient at the free surface and is numerically equal to unity. Its explicit inclusion in the formulas here is mainly for pedantic purposes. The other reflection coefficient symbols are defined in the text. For incident P, SH, and subcritical SV waves, all of these coefficients are real valued and independent of frequency. Hence, they may be used as time-domain scalars.

APPENDIX B
GEOPHONE EQUIVALENT CIRCUIT

The common electromechanical model of the moving-coil seismometer can be parameterized in terms of the seven constants ($M, f_0, h_{oc}, G, R_c, L_c, R_s$), where M = inertial mass, f_0 = natural frequency, h_{oc} = open circuit damping factor, G = transduction coefficient, R_c = coil resistance, L_c = coil self-inductance, and R_s = shunt resistance (see Figure B-1). Establishment of the Thévenin equivalent circuit for the geophone entails deriving expressions for an emf $E_{eq}(f)$ and a series impedance $Z_{eq}(f)$ in terms of these parameters that together exactly reproduce the transduction and loading properties of the real seismometer.

This standard geophone model can be augmented to account for the compliant coupling of the geophone to the ground (Hoover and O'Brien, 1980; Krohn, 1984). As indicated in Figure B-1, a simple spring and dashpot filter is inserted between the horizontal ground surface and the base of the seismometer. This is a phenomenological characterization of the complicated physical process of scattering of incident elastic waves by a small obstacle of finite mass and extent placed on a half-space surface. The mass and elastic medium form an oscillatory system that is excited by the incident pulse; damping of the oscillations is provided by reradiation of compressional, shear, and surface waves back into the half-space. The mechanical filter representing this

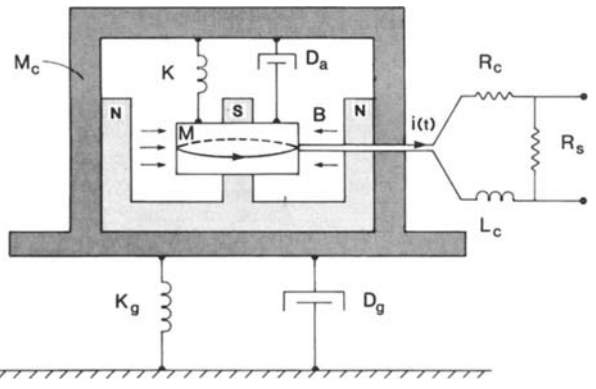

FIG. B-1. Geophone electromechanical model. Inertial mass M consists of a wire coil wound upon a conducting coil former and suspended within a radially directed magnetic field $\mathbf{B}$. K is elastic coefficient of spring suspension and D_a is viscous damping coefficient associated with air drag. Geophone natural angular frequency is $\omega_0 = \sqrt{K/M}$ and open circuit damping factor is $h_{oc} = h_a + h_e$, where h_a and h_e are damping factors associated with air drag and eddy current flow, respectively. Internal impedance to coil current $i(t)$ is provided by coil resistance R_c, coil self-inductance L_c, and shunt resistance R_s. Ground-coupling filter is characterized by geophone-case mass M_C, spring constant K_g, and viscous damping coefficient D_g.

process possesses a natural angular frequency ω_g and damping factor h_g given by

$$\omega_g^2 = \frac{K_g}{M_C} \tag{B-1}$$

and

$$h_g = \frac{D_g}{2M_C\omega_g}. \tag{B-2}$$

M_C is the mass of the geophone case (in the current context, the case consists of the plastic housing of the geophone and all other entities rigidly affixed thereto—magnet, pole pieces, spike or baseplate, cable anchors and takeouts, etc.). The frequency response of this ground-coupling filter is low-pass, high-cut, and exhibits a resonance in the vicinity of the natural frequency $f_g = \omega_g/2\pi$. The actual location of the resonance peak, as well as its height and width, are also controlled by the damping factor h_g.

If $U_z(f)$ is the (Fourier transformed) vertical component of the input ground-displacement function, then the Thévenin equivalent emf of the system shown in Figure B-1 is

$$E_{eq}(f) = \frac{R_s}{R_s + Z_c(f) + Z_{mot}(f)} \times \frac{G(i2\pi f)^2 P_4(f)}{P_1(f)P_2(f) + (M/M_C)(i2\pi f)^2 P_3(f)} (i2\pi f)U_z(f). \tag{B-3}$$

Polynomials in frequency f in this equation are given by

$$P_1(f) = (i2\pi f)^2 + 2h_{oc}\omega_0(i2\pi f) + \omega_0^2,$$

$$P_2(f) = (i2\pi f)^2 + 2h_g\omega_g(i2\pi f) + \omega_g^2,$$

$$P_3(f) = 2h_a\omega_0(i2\pi f) + \omega_0^2,$$

and

$$P_4(f) = 2h_g\omega_g(i2\pi f) + \omega_g^2.$$

$Z_c(f) = R_c + (i2\pi f)L_c$ is the electrical impedance of the geophone coil and $Z_{mot}(f)$ is the motional impedance of the suspended mass-case mass system (defined below). The frequency response of the system is defined as the open circuit output voltage divided by input ground velocity, or $E_{eq}(f)/(i2\pi f)U_z(f)$.

The Thévenin equivalent impedance of the seismometer and coupling filter system is

$$\frac{1}{Z_{eq}(f)} = \frac{1}{R_s} + \frac{1}{Z_c(f) + Z_{mot}(f)}, \tag{B-4}$$

i.e., a parallel combination of the shunt resistance R_s with the sum of the coil and motional impedances. The motional impedance is a generalization of the more familiar mass impedance $Z_M(f)$ associated with an electrodynamic seismometer:

$$Z_{mot}(f) = \frac{P_1(f)P_2(f)}{P_1(f)P_2(f) + (M/M_C)(i2\pi f)^2 P_3(f)} Z_M(f). \tag{B-5}$$

$Z_M(f)$ is given in turn by $(i2\pi f)G^2/MP_1(f)$ and can be interpreted as the impedance of a parallel RLC circuit. Obviously, the generalization of equation (B-5) is significant only to the extent that the suspended mass-case mass ratio is nonnegligible.

Incorporation of the ground coupling filter into the basic theoretical description of the seismometer means that four additional parameters (f_g, h_g, M/M_C, h_a) are required to specify geophone behavior. For the current generation of seismic-reflection geophones, M/M_C and h_a can probably be neglected; the extended parameter set then consists of nine constants. Values of these parameters may, in general, vary among individual geophones of a group. Hence, each of the parameters appearing in the expressions for $E_{eq}(f)$ and $Z_{eq}(f)$ above should be subscripted with the two group connection indices $i(n)$ and $j(n)$ introduced in the text. Finally, although the derivation of the Thévenin equivalent circuit has employed the assumption that the geophone is vertically oriented and placed on a half-space surface, the results are also considered valid for nonvertical geophones located on or within an elastic medium. The input signal becomes the component of elastic particle velocity at the geophone location that is parallel to the geophone sensitivity axis. In the frequency domain, this component is $(i2\pi f)\mathbf{a}_n \cdot \mathbf{U}(\mathbf{r}_n, f)$ where $\mathbf{U}(\mathbf{r}, f)$ is the Fourier transform of the elastic particle displacement $\mathbf{u}(\mathbf{r}, t)$.

APPENDIX C

GROUP LOAD IMPEDANCE AND TRANSMISSION LINE TRANSFER FACTOR

With modern distributed data acquisition instrumentation, much or all of the recording-system electronics is deployed physically near the seismometer group. In such situations, the transmission line connecting group to recording system may be electrically modeled as a purely resistive cable pair possessing lumped line resistance R_L. The group load impedance Z_L and the voltage transfer factor T assume simple forms. If Z_R is the input impedance of the recording system, then

$$Z_L = Z_R + R_L, \tag{C-1}$$

$$T = \frac{E_R}{E_L} = \frac{Z_R}{Z_R + R_L}. \tag{C-2}$$

Obviously, for a high input impedance system, $Z_L \approx Z_R$ and $T \approx 1$. A more conventional data-acquisition setup uses a long transmission line to connect the geophone group with a remote recording cab. The filtering and loading effects of this cable should not be ignored, particularly at the higher frequency ranges. The cable can be electrically modeled as a continuously distributed series impedance and shunt conductance. Classical transmission line theory yields expressions for the load impedance Z_L and voltage transfer factor T appropriate for this configuration.

Lindsey (1971) has emphasized that the transmission line used for much conventional seismic data acquisition should be considered an integral part of the field-filtering hardware.

A geophone group is typically connected across a wire pair of a multiconductor CDP cable at some point intermediate between its two ends. One end of the cable is loaded with the input impedance of the recording system Z_R, while the other end is shunted with a terminator impedance Z_T (Z_T may be infinite). The electrical transmission properties of the cable itself are determined by its characteristic impedance Z_0 and propagation constant γ.

Let Z_1 be the input impedance of the loaded transmission line looking from the geophone group terminals toward the recording system and Z_2 be the input impedance looking from this same point toward the terminator. Then, the total load impedance Z_L presented to the geophone group by the transmission line/recording system/terminator configuration of Figure C-1 is the parallel combination of Z_1 and Z_2: $Z_L = (Z_1 Z_2)/(Z_1 + Z_2)$. Z_1 depends upon the distance d_R to the recording system in the following manner:

$$Z_1 = Z_0\left[\frac{Z_R \cosh(\gamma d_R) + Z_0 \sinh(\gamma d_R)}{Z_R \sinh(\gamma d_R) + Z_0 \cosh(\gamma d_R)}\right]. \quad \text{(C-3)}$$

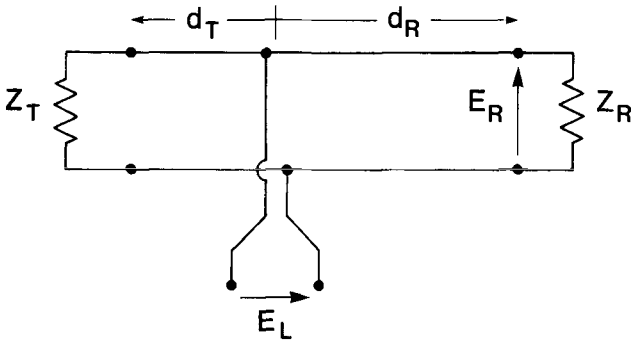

FIG. C-1. Electrical configuration of a conventional seismic recording channel.

Z_2 is given by an analogous formula where d_T and Z_T replace d_R and Z_R, respectively.

The transmission-line transfer factor T is defined as the ratio of output to input voltage. In the present context, the input is the voltage E_L generated by the geophone group across its total load impedance, while the output is the voltage E_R appearing at the recording system. Hence

$$T = \frac{E_R}{E_L} = \frac{Z_R}{Z_R \cosh(\gamma d_R) + Z_0 \sinh(\gamma d_R)}. \quad \text{(C-4)}$$

The characteristic impedance and propagation constant can be determined by direct measurement of the open- and short-circuit impedances of a length d of CDP cable:

$$Z_0 = \sqrt{Z_{sc} Z_{oc}} \quad \text{(C-5)}$$

and

$$\tanh(\gamma d) = \sqrt{\frac{Z_{sc}}{Z_{oc}}}. \quad \text{(C-6)}$$

Alternatively, if field measurements of these quantities are not available, Z_0 and γ can be determined by evaluating their defining formulas with suitable estimates of the cable electrical parameters:

$$Z_0^2 = \frac{r + (i2\pi f)\ell}{s + (i2\pi f)c} \quad \text{(C-7)}$$

and

$$\gamma^2 = [r + (i2\pi f)\ell][s + (i2\pi f)c], \quad \text{(C-8)}$$

where r = series resistance per unit length, ℓ = series inductance per unit length, s = shunt conductance per unit length, and c = shunt capacitance per unit length. Often, the effects of ℓ and s are negligible in the seismic frequency band (Lindsey, 1971; Berni and Parrish, 1981; Smither and Khan, 1983).